A Shortcut Pressure Swing Adsorption Analogue Model to Estimate Gas-in-Place and CO_2 Storage Potential of Gas Shales

Humera Ansari[a], Elena Rietmann[a], Lisa Joss[b], JP Martin Trusler[a], Geoffrey Maitland[a], Ronny Pini[a,*]

[a] *Department of Chemical Engineering, Imperial College London, London, SW7 2AZ, UK*
[b] *Department of Chemical Engineering and Analytical Science, The University of Manchester, Manchester, M13 9PL, UK*

Abstract

Natural gas extraction from shale formations has experienced a rapid growth in recent years, but the low recovery observed in many field operations demonstrates that the development of this energy resource is far from being optimal. The ambiguity in procedures that account for gas adsorption in Gas-in-Place calculations represents an important element of uncertainty. Here, we present a methodology to compute gas production curves based on quantities that are directly accessed experimentally, so as to correctly account for the usable pore-space in shale. We observe that adsorption does not necessarily sustain a larger gas production compared to a non-adsorbing reservoir with the same porosity. By analysing the entire production curve, from initial to abandonment pressure, we unravel the role of the excess adsorption isotherm in driving this behaviour. To evaluate scenarios of improved recovery by means of gas injection, we develop a proxy reservoir model that exploits the concept of Pressure Swing Adsorption used in industrial gas separation operations. The model has three stages (Injection/Soak/Production) and is used to compare scenarios with cyclic injection of CO_2 or N_2. The result show that partial pressure and competitive adsorption enhance gas production in complementary ways, and reveal the important trade-off between CH_4 recovery and CO_2 storage. In this context, this proxy model represents a useful to tool to explore strategies that optimise these quantities without compromising the purity of the produced stream, as the latter may introduce a heavy economic burden on the operation.

Keywords: GIP, Gas Adsorption, Carbon Storage, Shale

*Corresponding author
Email address: r.pini@imperial.ac.uk (Ronny Pini)

1. Introduction

Due to the rising global demand of natural gas, the interest in unconventional gas resources, such as gas shales, has recently grown [1]. Progress in production techniques, such as hydraulic fracturing and horizontal drilling, is allowing access to massive reserves of natural gas [2, 3, 4]. In conventional reservoirs, natural gas exists mostly as compressed supercritical fluid in pores and fractures and its behaviour is described by a suitable equation of state. Shales, on the other hand, have very small pores (nanometric in size), where gas can densify as a result of physical adsorption [5]. While the presence of nano-scale pores enhances storage capacity by retaining gas at liquid-like densities [6], it also introduces severe limitations to mass transfer in terms of low (nano-Darcy) permeability [7]. Production from shale formations starts to decline in less than 3–4 years from initial production and recovery factors from these reservoirs are low, usually ranging from 1–30% [8, 9]. In so-called conventional reservoirs, secondary recovery methods are routinely used to sustain productivity. By analogy with coal-bed methane recovery [10], reservoir engineering practices can be considered for shale, whereby gas is injected into the formation to sustain a pressure gradient, while reducing the partial pressure of methane and increasing its extraction. When CO_2 is used as the injected gas, it can be retained in the formation by the same mechanisms that led to the accumulation of natural gas, thereby reducing the impact of hydrocarbon production on climate change. Shale plays are usually significant in size, providing a potentially large CO_2 sequestration site [11, 12]. The coupling of gas recovery with CO_2 injection and storage also poses many operational benefits, including the utilisation of existing infrastructure to achieve higher recovery rates [13], and the maintenance of reservoir pressure to limit the risk of subsidence [14].

CO_2-Enhanced Shale Gas Recovery (CO_2-ESGR) has been considered to have great economic potential - 71 trillion m^3 additional CH_4 recovery, while providing 280 Gt of CO_2 storage [15]. A few modelling studies have evaluated the potential of specific shale plays. Tao and Clarens (2013) estimated that the Marcellus Shale would be able to store 10.4–18.4 Gt of CO_2 by 2030 based on the CH_4 production rates [13]. Similarly, Edwards et al. (2015), found storage capacities of 7.2–9.6 Gt for the Marcellus shale and 2.1–3.1 Gt for the Barnett Shale [16]. Li and Elsworth (2015) showed an enhanced recovery between 2–29% depending on the CO_2 injection strategy [12]. Practical demonstration of *in-situ* CO_2 injections are quite rare however. In a small-scale trial, around 500 tons of CO_2 were injected in a shale reservoir located in the Morgan County, Tennessee (USA) and results showed that after an initial soaking period, the daily average production rate of hydrocarbons from the well increased compared to data before CO_2 injection [17].

There are still outstanding questions that remain to be answered about ESGR. To list a few: How could such a cyclic operation be implemented in practice given the low permeability of shale? What would be the optimum pressure to operate such a process? Is there an injection scheme that maximises recovery and storage simultaneously? Answering these questions requires understanding the gas adsorption properties of shale at the elevated pressure and temperature conditions found in the formation. CO_2-ESGR is in fact founded upon the principle that CO_2 adsorbs preferentially within the rock as compared to CH_4 [11, 16]. While experimental studies have confirmed a favourable adsorption selectivity towards CO_2 [18, 19], the use of the same experimental adsorption quantities in volumetric calculations for storage capacity estimation has not yet been addressed properly. As discussed in the next section, a key element in the analysis is the use of the so-called excess amount adsorbed, which is the truly measurable quantity in a high-pressure gas adsorption experiment.

In this paper we develop and deploy a simplified mathematical model that exploits the concept of Pressure Swing Adsorption (PSA), as used in industrial gas separations, to describe an ESGR operation that involves three stages: Injection, Soak and Production. The model framework is built entirely on material balances and uses quantities that can be directly accessed experimentally, so as to correctly account for the pore-space occupancy in shale. We evaluate CO_2 and N_2 as injection gases and identify a number of operational constraints and strategies.

2. Background: Supercritical Gas Adsorption in Shale

The Gas-in-Place (GIP) is a metric that dictates a reservoir's suitability for production and the design of an optimum production strategy must rely on the knowledge of how GIP varies as a function of reservoir pressure. There are three main ways in which gas is stored in shales: (1) adsorption on the organic matter and the clay minerals; (2) compression as free gas in pores and fractures; and (3) dissolution in formation fluids (oil and water) [20, 21, 22]. The relative proportion of each mechanism varies from shale to shale, with adsorption contributing to 20–85% of GIP [23, 24, 25]. Common approaches to estimate GIP for shales do account for the mass of adsorbed gas, but they neglect its volume by assuming that the total rock's porosity continues to be available to the free gas [26, 27, 28]. It has been reported that this assumption can lead to an overestimation of the actual GIP by approximately 10–25% [27]. The reliability of this excercise is further compromised by the fact that the distinct dependency of gas bulk density and adsorption capacity on pressure is not accounted for. As anticipated below and described in Section 3, the use of excess adsorption

quantities in GIP calculations circumvents the problem by correctly accounting for the usable porosity, while avoiding unnecessary assumptions on the properties of the adsorbed phase and their dependency on the pressure. We note that these complications are largely due to the fact that shale is mostly mesoporous, implying that adsorbed and free gas occupy the same pore space. Filling this pore space with compressed gas and additionally accounting for adsorption leads to double counting. This is in contrast with another natural adsorbent, coal, which is largely microporous and enables the "simpler" allocation of the adsorbed and free gas phases between the micro- and macro-porous space, respectively.

At the typical shale reservoir conditions, both CH_4 and CO_2 are supercritical. Because of the absence of a vapour-liquid transition, adsorption measurements of supercritical gases are interpreted using excess quantities. The so-called excess amount adsorbed refers to the amount of fluid that exists in the pores *in excess* of the fluid which would exist there at the same temperature and pressure in the absence of adsorption (i.e. as a bulk fluid) [29]. The excess CH_4 adsorption capacity has been observed to range between 3–8 $\mathrm{m}^3_{\mathrm{STP}}/\mathrm{m}^3$ for shales from the Barnett, New Albany and Woodford formations [30, 31, 32, 25, 18]. Experimental CO_2 adsorption data on shale are scarcer and more scattered [33], with only a few studies reporting data at sufficiently high pressures (> 10 MPa), indicating excess adsorption capacities of 8–10 $\mathrm{m}^3_{\mathrm{STP}}/\mathrm{m}^3$ [30, 18]. While the excess amount adsorbed is the measured property experimentally, the practitioner often chooses to convert it to an absolute amount adsorbed for the purpose of process modelling. This conversion requires an assumption on the density (or volume) of the adsorbed phase. For a pure gas, the conversion is given by the following expression:

$$n_{\mathrm{ex}} = n_{\mathrm{a}} - \rho_{\mathrm{b}} v_{\mathrm{a}} = n_{\mathrm{a}} \left(1 - \frac{\rho_{\mathrm{b}}}{\rho_{\mathrm{a}}}\right) \tag{1}$$

where n_{ex} and n_{a} are the excess and absolute amount adsorbed, respectively, ρ_{b} is the bulk density of the gas, v_{a} is the volume of the adsorbed phase and $\rho_{\mathrm{a}} = n_{\mathrm{a}}/v_{\mathrm{a}}$ is the density of the adsorbed phase. Figure 1 shows (a) excess CH_4 adsorption isotherms and (b) their absolute counterparts, obtained upon assuming a liquid-like adsorbed phase with a density $\rho_{\mathrm{a}} = 22.3$ mol/L. For the sake of generality, four common adsorption isotherm models are considered in the figure (equations provided in the Supplementary Information), which prompt the following remarks. First, the absolute amount adsorbed always increases with pressure, while the excess can feature a non-monotonic behaviour (e.g. Langmuir isotherm). The latter does not indicate a decrease in adsorption, but rather a decrease of its contribution to the total amount of gas stored in the porous rock. Secondly, $n_{\mathrm{ex}} \leq n_{\mathrm{a}}$ over the entire pressure range, with the relative difference between the

two quantities that increases with increasing pressure ($n_{ex} \approx n_a$ at $P < 4$–5 MPa). It becomes apparent from these initial considerations that the use of absolute instead of excess quantities in material balance calculations will produce different results, if the volume occupied by the adsorbed phase is not accounted for.

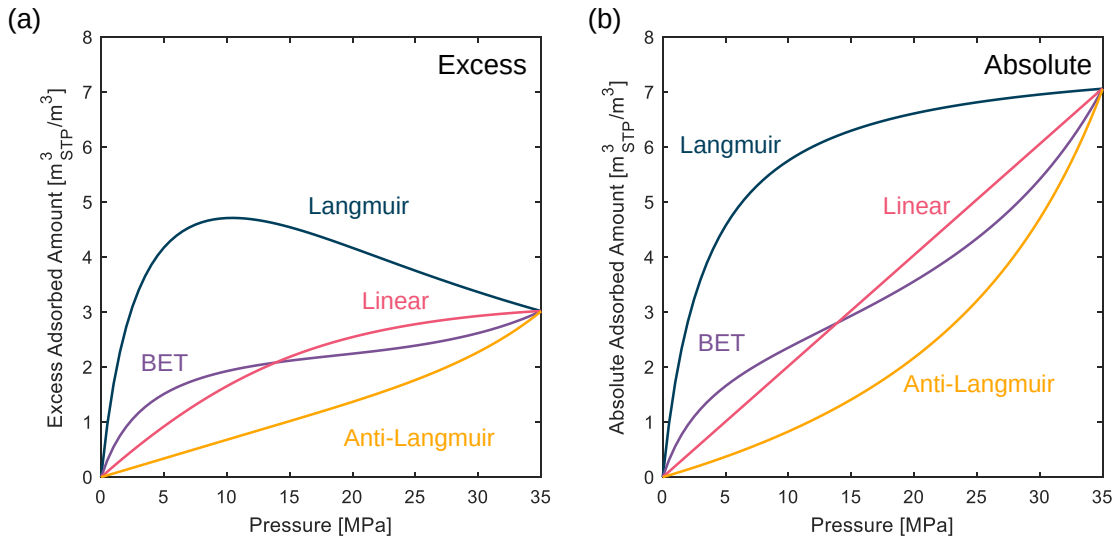

Figure 1: CH_4 (a) excess and (b) absolute adsorption isotherms as a function of pressure, as predicted using four adsorption isotherm models, namely the Langmuir, Anti-Langmuir, BET and Linear model. The equations and parameters of each model are provided in the Supplementary Information.

In this study, we will also consider an enhanced recovery operation, in which a gas is injected into the formation to displace natural gas, thereby creating a binary gas mixture. In this case, absolute and excess adsorption are related as follows [34]:

$$n_{i,\mathrm{ex}} = n_{i,\mathrm{a}}\left(1 - \frac{y_i C_\mathrm{t}}{z_i \overline{\rho}_\mathrm{a}}\right) \tag{2}$$

where C_t is the total concentration of the bulk phase, $\overline{\rho}_\mathrm{a}$ is the adsorbed phase density of the gas mixture, y_i is the mole fraction of component i in the bulk phase and z_i ($z_i = n_{i,\mathrm{a}} / \sum_i n_{i,\mathrm{a}}$) is the mole fraction of component i in the adsorbed phase. The density of the adsorbed phase, $\overline{\rho}_\mathrm{a}$, can be estimated by assuming ideal mixing [35]:

$$\overline{\rho}_\mathrm{a} = \left(\sum_i \frac{z_i}{\rho_{i,\mathrm{a}}}\right)^{-1} \tag{3}$$

The volume of the adsorbed phase is then calculated as follows:

$$\overline{v}_{\mathrm{a}} = \frac{n_{i,\mathrm{a}}}{z_i \overline{\rho}_{\mathrm{a}}} \tag{4}$$

The amount of component i adsorbed, $n_{i,\mathrm{a}}$, from the multicomponent gas mixture can be predicted by various means, including thermodynamic approaches (e.g. the Real Adsorbed Solution Theory, RAST) or an appropriate extension of the single-component adsorption isotherm model, such as the extended Langmuir model. The availability of closed-form expressions to predict mixed-gas adsorption equilibria is often used as the argument for choosing the latter option in process optimisation calculations, such as those used to describe cyclic adsorption processes [36].

3. Shortcut Pressure Swing Adsorption Analogue model

The proposed model concept is inspired from industrial gas adsorption separations, in which a porous adsorber undergoes cyclically a pressurisation ("adsorption") and de-pressurisation ("desorption") step. Proxy models that assume uniform conditions throughout the system have been shown to provide a useful means to rationalise the results arising from the analysis of such cyclic operation, while simplifying considerably the mathematical formulation of the problem [37]. We will follow a similar approach in this study to evaluate the exploitation of a shale reservoir that is accessed by wells from which gas is injected and withdrawn. The process is thus reminiscent of a 'huff-n-puff' operation [38, 39, 40], but is extended here to a situation where multiple injection-recovery cycles are carried out, so as to elucidate potential trade-offs between incremental recovery, produced gas quality and gas storage. In our conceptualisation, the following assumptions apply:

- The system is well-mixed, and there are no pressure, concentration or temperature gradients in the system;
- Shale properties, such as porosity and adsorption parameters, are constant throughout the reservoir;
- Formation water is considered to be immobile and is not accounted for in the reservoir porosity;
- The system is isothermal;
- Natural gas is represented by pure methane, CH_4.

The cyclic operation has three distinct stages (Figure 2): Injection (I) − where gas is introduced in the reservoir; Soak (S) − where adsorption equilibrium is reached between fluid and solid phase; and Production

(R) − where either CH_4 or a mixture of CH_4 and the injected gas are produced. In the latter case, the two components are separated, and as the cycle continues, the gas is then re-injected into the reservoir in the following Injection stage. The assumption of a well-mixed reservoir presents a deviation from the expected behaviour in the shale reservoir. There, the finite spacing between natural and artificial fractures will limit the achievable rate of mass transfer, meaning that the well would need to be shut in for a sufficiently long time in order to reach adsorption equilibrium during the Soak stage. In fact, mass transfer rates have a major impact on the achievable gas quality and recovery. In the following, we outline the mathematical formulation of the model, including the performance indicators for the gas recovery/storage operation.

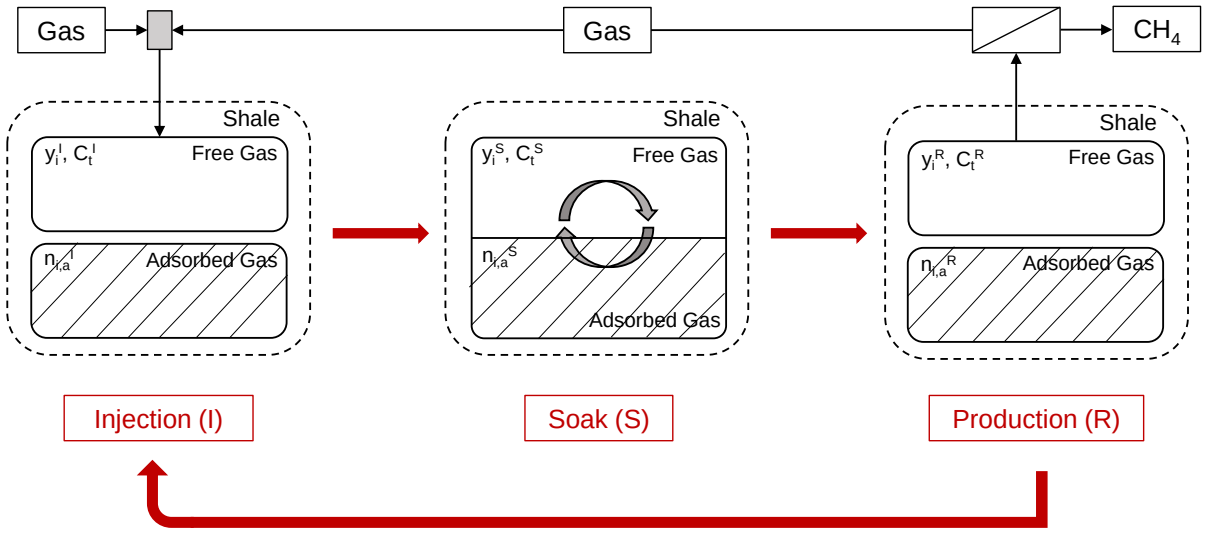

Figure 2: Schematic of the cyclic shale production and storage model.

3.1. Mathematical Model

The total amount of component i (in moles) in the reservoir at a given stage is $N_{i,\mathrm{t}}$, which includes contributions from the free gas, FG, ($N_{i,\mathrm{f}}$) and the adsorbed phase, AG, ($N_{i,\mathrm{a}}$):

$$N_{i,\mathrm{t}} = N_{i,\mathrm{f}} + N_{i,\mathrm{a}} \tag{5}$$

where,

$$N_{i,\mathrm{f}} = V y_i C_{\mathrm{t}} (\phi - \rho_{\mathrm{w,s}} v_{\mathrm{a}}) \tag{6}$$

$$N_{i,\mathrm{a}} = V \rho_{\mathrm{w,s}} n_{i,\mathrm{a}} \tag{7}$$

In Eqs. 6 and 7, y_i is the bulk gas phase mole fraction of component i, ϕ is the total reservoir porosity, C_t is the total concentration of the bulk phase (in mol/m^3), V is the volume of the reservoir (in m^3), $\rho_{\mathrm{w,s}}$ is the bulk density of the reservoir (in kg/m^3), v_a is the specific volume of the adsorbed phase (in m^3/kg) and $n_{i,\mathrm{a}} = f(y_i, P, T)$, is the absolute amount adsorbed per unit mass of shale (in mol/kg). The second term in Eq. 6 accounts for the volume occupied by the adsorbed phase and therefore, for the reduction in porosity available to the free gas. By using the definitions introduced in Section 2, Eq. 5 can be recast as:

$$N_{i,\mathrm{t}} = V(\phi y_i C_\mathrm{t} + \rho_{\mathrm{w,s}} n_{i,\mathrm{ex}}) \tag{8}$$

The recoverable amount of component i in the reservoir, $G_{i,\mathrm{t}}$, is more conveniently expressed using units of standard volume ($\mathrm{m}^3_{\mathrm{STP}}/\mathrm{m}^3$):

$$G_{i,\mathrm{t}} = \frac{1}{\rho_{\mathrm{sc}}} \left(\phi y_i C_\mathrm{t} + \rho_{\mathrm{w,s}} n_{i,\mathrm{ex}} \right) \tag{9}$$

where ρ_{sc} is the density of the fluid at standard conditions (1 atm and 0 °C). Eq. 9 predicts the amount of recoverable gas purely based on the achieved production pressure. Therefore, it neglects reductions in the recoverable volume that may be caused by practical limitations and/or other physical processes, which are commonly accounted for by means of so-called efficiency factors [41]. We also note that the conventional method of calculating the GIP uses $n_{i,\mathrm{a}}$ instead of $n_{i,\mathrm{ex}}$ in Eq. 9, thereby overestimating the porosity accessed by the free gas. We will compare both methodologies in this work.

Traditionally, material balance calculations for primary recovery operations (no injection, single-component gas) use a graphical approach, where the recoverable volume of gas (corresponding to the GIP) is plotted as a function of P/Z (Z is the fluid compressibility) [42]. Mathematically:

$$\mathrm{GIP} = G_\mathrm{t} = \frac{1}{\rho_{\mathrm{sc}}} \left(\frac{\phi}{RT} \frac{P}{Z} + \rho_{\mathrm{w,s}} n_{\mathrm{ex}} \right) \tag{10}$$

where R is the universal gas constant and T is the reservoir temperature. The amount of gas produced at a

given reservoir pressure, P, is thus estimated as:

$$G_{\mathrm{p}} = G_{\mathrm{t},0} - \mathrm{GIP} \tag{11}$$

where $G_{\mathrm{t},0}$ is the original GIP (OGIP). For a so-called volumetric reservoir (no adsorption), the OGIP can be readily estimated from production data by extrapolation to $P/Z = 0$, because Eq. 11 represents a straight-line. In the presence of adsorption, the production data deviate from linearity [42]; because the strength of the deviation ultimately depends on the amount of gas desorbed, the accurate description of experimental adsorption data is key to obtain reliable estimates of the GIP during primary production.

For enhanced recovery by gas injection, we consider a cyclic operation, where each cycle starts with the Injection stage, followed by the Soak and Production stages (Figure 2). We note that the free and adsorbed gas phase are in equilibrium only in the Soak stage, meaning that only the free gas participates in the Injection and Production stages. This choice is motivated by the very low permeability of the unfractured rock matrix. The governing equations for each stage in a generic cycle j are described in the following sections. We refer to CH_4 with the subscript 'm' and the injected gas with subscript 'g'. The operation starts by depressurising the reservoir from the initial reservoir pressure, P_0, to the production pressure, P_{L}, after which the cyclic operation commences.

3.1.1. Injection Stage

At the start of the cycle (initial state 'R'), the reservoir is not under equilibrium, as it is straight after the initial depressurisation or a Production stage. A fixed amount, $N^{j}_{\mathrm{g,inj}}$, of pure gas (CO_2 or N_2) is injected into the reservoir (final state 'I'). The gas is only injected into the free phase (subscript 'f'), and the adsorbed phase (subscript 'a') remains unchanged. Only the amount of the injected component changes in the FG, while the amount of methane remains constant:

$$N^{\mathrm{I},j}_{i,\mathrm{a}} = N^{\mathrm{R},j-1}_{i,\mathrm{a}} \tag{12a}$$

$$N^{\mathrm{I},j}_{\mathrm{m,f}} = N^{\mathrm{R},j-1}_{\mathrm{m,f}} \tag{12b}$$

$$N^{\mathrm{I},j}_{\mathrm{g,f}} = N^{\mathrm{R},j-1}_{\mathrm{g,f}} + N^{j}_{\mathrm{g,inj}} \tag{12c}$$

where j refers to the injection cycle. The composition, pressure and total concentration of the bulk phase is then given by:

$$y_i^{\mathrm{I},j} = N_{i,\mathrm{f}}^{\mathrm{I},j} / N_{\mathrm{t,f}}^{\mathrm{I},j} \tag{13a}$$

$$C_{\mathrm{t}}^{\mathrm{I},j} = \frac{\rho_{\mathrm{w,s}} N_{\mathrm{t,f}}^{\mathrm{I},j}}{\phi - \rho_{\mathrm{w,s}} \overline{v}_{\mathrm{a}}^{\mathrm{R},j-1}} \tag{13b}$$

$$P^{\mathrm{I},j} = P(y_i^{\mathrm{I},j}, C_{\mathrm{t}}^{\mathrm{I},j}, T) \tag{13c}$$

where Eq. 13c denotes an equation-of-state. Eqs. 12 and 13 are only valid for $j > 1$. When $j = 1$, the reservoir comprises only of pure CH_4 and the following equations apply:

$$N_{\mathrm{m,a}}^{\mathrm{I},1} = N_{\mathrm{m,a}}^{0} \tag{14a}$$

$$N_{\mathrm{g,a}}^{\mathrm{I},1} = 0 \tag{14b}$$

$$N_{\mathrm{m,f}}^{\mathrm{I},1} = V C_{\mathrm{t}}|_{P_{\mathrm{L}}} (\phi - \rho_{\mathrm{w,s}} v_{\mathrm{a}}^{0}) \tag{14c}$$

$$N_{\mathrm{g,f}}^{\mathrm{I},1} = N_{\mathrm{g,inj}}^{1} \tag{14d}$$

where the superscript '0' refers to the initial reservoir conditions.

3.1.2. Soak Stage

After injection, a Soak stage (state 'S') is carried out to let the reservoir gases reach adsorption equilibrium. The following set of equations that describes the total and component mass conservation has to be solved simultaneously:

$$N_{\mathrm{m,a}}^{\mathrm{S},j} + N_{\mathrm{g,a}}^{\mathrm{S},j} + N_{\mathrm{m,f}}^{\mathrm{S},j} + N_{\mathrm{g,f}}^{\mathrm{S},j} = N_{\mathrm{m,a}}^{\mathrm{I},j} + N_{\mathrm{g,a}}^{\mathrm{I},j} + N_{\mathrm{m,f}}^{\mathrm{I},j} + N_{\mathrm{g,f}}^{\mathrm{I},j} \tag{15a}$$

$$N_{\mathrm{g,a}}^{\mathrm{S},j} + N_{\mathrm{g,f}}^{\mathrm{S},j} = N_{\mathrm{g,a}}^{\mathrm{I},j} + N_{\mathrm{g,f}}^{\mathrm{I},j} \tag{15b}$$

where,

$$N_{i,\mathrm{a}}^{\mathrm{S},j} = V\rho_{\mathrm{w,s}} n_{i,\mathrm{a}}(y_i^{\mathrm{S},j}, C_{\mathrm{t}}^{\mathrm{S},j}) \tag{16a}$$

$$N_{i,\mathrm{f}}^{\mathrm{S},j} = V y_i^{\mathrm{S},j} C_{\mathrm{t}}^{\mathrm{S},j}(\phi - \rho_{\mathrm{w,s}} v_{\mathrm{a}}^{\mathrm{S},j}) \tag{16b}$$

The two unknowns are the equilibrium bulk phase composition ($y_i^{\mathrm{S},j}$) and the total concentration of the bulk phase ($C_{\mathrm{t}}^{\mathrm{S},j}$). The pressure at the end of the Soak stage is calculated using an equation-of-state:

$$P^{\mathrm{S},j} = P(y_i^{\mathrm{S},j}, C_{\mathrm{t}}^{\mathrm{S},j}, T) \tag{17}$$

3.1.3. Production Stage

At the start of the Production stage, the reservoir is at equilibrium at a given pressure, $P^{\mathrm{S},j}$, and bulk composition, $y_i^{\mathrm{S},j}$. Gas production is carried out by reducing the reservoir pressure to the specified level, P_{L}. This process is not at equilibrium; while gas is withdrawn from the free bulk phase, the adsorbed phase remains unaffected. The following equations describe the amount of FG and AG at the end of this stage (final state 'R'):

$$N_{i,\mathrm{a}}^{\mathrm{R},j} = N_{i,\mathrm{a}}^{\mathrm{S},j} \tag{18a}$$

$$N_{i,\mathrm{f}}^{\mathrm{R},j} = V y_i^{\mathrm{S},j} C_{\mathrm{t}}^{\mathrm{R},j}|_{P_{\mathrm{L}}}(\phi - \rho_{\mathrm{w,s}} \overline{v}_{\mathrm{a}}^{\mathrm{S},j}) \tag{18b}$$

$$N_{i,\mathrm{prod}}^{j} = N_{i,\mathrm{f}}^{\mathrm{S},j} - N_{i,\mathrm{f}}^{\mathrm{R},j} \tag{18c}$$

Eq. 18c is used to compute the amount of component i that is produced. For the first depressurisation, prior to the first Injection stage, the amount of methane gas produced is $N_{\mathrm{m,prod}}^{0} = V(C_{\mathrm{t}}|_{P_0} - C_{\mathrm{t}}|_{P_{\mathrm{L}}})(\phi - \rho_{\mathrm{w,s}} v_{\mathrm{a}}^{0})$. After the final Production stage, the reservoir is abandoned; there is a final Soak stage, where the reservoir re-equilibrates.

3.1.4. Solution Procedure

The cyclic operation of the reservoir starts and ends at state 'R', passing through the 'I' and 'S' stages. The design variables are P_{L}, $N_{\mathrm{g,inj}}^{j}$ and the total number of injections, J. It is worth noting that while the absolute amount adsorbed remains constant during injection and production stages, the excess amount

adsorbed may vary, because it depends on the amount of gas in the free bulk phase. The mathematical model was implemented in MATLAB R2020a and the set of nonlinear equations (Eqs. 15 and 16) was solved using `lsqnonlin` with a tolerance of $1x10^{-9}$ and the default of 400 iterations. A NIST REFPROP [43] MATLAB wrapper was used for the equation-of-state for each fluid and/or their mixtures.

3.2. Model Parameters

The Marcellus shale is the largest shale play in the USA [44] and has about 135 trillion cubic feet of proven reserves [45]. In this work, we use the physical properties of this shale reservoir to demonstrate the applicability of the shortcut PSA analogue model. Reservoir properties and operational parameters are reported in Table 1. Either pure CO_2 or N_2 is injected to displace the resident gas, which is initially pure methane. Five injection cycles are conducted by introducing a constant volume of gas at each injection stage, corresponding to approximately 100 times the pore volume of the reservoir. In the model, excess adsorption isotherms are generated from the corresponding absolute quantity by assuming a constant adsorbed phase density. For each fluid, the latter takes the value of the density of the saturated liquid at 35 MPa (Table 2); this reflects common pore densities found in the literature for shale reservoirs [46, 30].

Table 1: Model parameters, including reservoir properties and operational parameters.

Parameter	Value	Source
Initial Reservoir Pressure, P_0	35 MPa	[44, 47, 48]
Reservoir Temperature, T	55 °C	[44, 47, 48]
Reservoir Porosity, ϕ	8%	[49]
Reservoir Bulk Density, $\rho_{\mathrm{w,s}}$	2,550 kg/m^3	[50]
Production Pressure, P_{L}	10 MPa	–
Number of Cycles, J	5	–
Gas Injected per Cycle, $N_{\mathrm{g,inj}}/V$	357 mol/m^3	–

Table 2: The adsorbed phase density (ρ_{a}) and density at standard conditions (ρ_{sc}) for each fluid in this work. [a] Liquid density at 35 MPa and 190 K (CH_4), 303 K (CO_2) and 124 K (N_2).

Gas	CH_4	CO_2	N_2	Source
ρ_{a} (mol/m^3)[a]	22,342	21,996	25,821	[51]
ρ_{sc} (mol/m^3)	44.135	44.326	44.635	[51]

The model is solved by providing the constitutive equation for a given adsorption isotherm model, $n_{i,\mathrm{a}} = f(y_i, P, T)$. The four models selected for this study are shown in Figure 1 and include the Langmuir, the BET, the Linear and the Anti-Langmuir model. The equations for each model are provided in the Supplementary

Information, together with the model parameters. The first two models have been used previously to describe adsorption on shale and coal [32, 52, 48], while the last two have been added here for the sake of generality. The isotherms have been constructed such that the absolute adsorbed amount at P_0 (35 MPa) is equal for all adsorption models, namely 5 kg/m^3 for CH_4, as shown in Figure 1. For the ESGR process, the mixed-gas adsorption equilibrium is described using the extended Langmuir model formulated for two components (i and k):

$$n_{i,\mathrm{a}} = \frac{n^{\max} K_i P y_i}{1 + K_i P y_i + K_k P y_k} \tag{19}$$

where K_i and K_k are the pure component Langmuir parameters for component i and k, respectively (values provided in the Supplementary Information). We note that to ensure thermodynamic consistency, the molar saturation capacity, $n^{\max}$, is the same for each component in the mixture, meaning that the selectivity of species i relative to species k for any bulk phase composition and pressure is simply the ratio of the Langmuir parameters, K_i/K_k. The extended Langmuir model was used in this study for its simplicity, but the approach may be easily adapted to the use of more complex theories, such as RAST. In fact, while these two approaches have been shown to produce similar composition fronts during cyclic adsorption processes, RAST may be needed to improve the agreement between the experimental and modelling results [53].

3.2.1. Performance Metrics

The two main parameters that are of interest in an ESGR process are (i) the total recovery of CH_4 and (ii) the total amount of injected gas that remains in the reservoir after abandonment (storage). The Enhanced Recovery factor is defined as the ratio between the total amount of CH_4 produced with enhanced recovery and the amount of CH_4 that would have been produced from primary recovery by depressurisation to the same pressure (P_{L}), but without any gas injection ($N_{\mathrm{m,PR}}$):

$$R_{\mathrm{m}} = \frac{N^0_{\mathrm{m,prod}} + \sum_{j=1}^{J} N^j_{\mathrm{m,prod}}}{N_{\mathrm{m,PR}}} \tag{20}$$

The Storage factor is defined as the ratio between the total number of moles of the injected gas left in the reservoir at the end of cycle J and the cumulative amount of gas injected into the reservoir:

$$S_{\mathrm{g}} = \frac{N_{\mathrm{g,t}}^{J}}{\sum_{j=1}^{J} N_{\mathrm{g,inj}}^{j}} \tag{21}$$

4. Results

The following section is divided into two main parts: (1) *Primary recovery*, where the impact of different adsorption isotherm models is investigated by evaluating the $P/Z - G_{\mathrm{p}}$ curves for a recovery operation driven exclusively by depressurisation; and (2) *Recovery with gas injection*, where the use of two different gases with opposite selectivity relative to CH_4 is assessed, namely CO_2 and N_2; to this end, only the extended Langmuir adsorption isotherm model will be considered, because of its proven general applicability.

4.1. Primary Recovery by Depressurisation

4.1.1. GIP and Initial Reservoir Pressure

It is highly instructive to first investigate the $P/Z - G_{\mathrm{p}}$ diagram for the case of the Langmuir adsorption isotherm model, as shown in Figure 3a for four initial reservoir pressures, P_0. Three sets of curves are plotted to represent three contrasting cases, namely: (i) no adsorption ("base case", dashed straight line); (ii) adsorption without porosity correction ("absolute", light blue); and (iii) adsorption with porosity correction ("excess", dark blue). The latter is the true cumulative gas production curve for an adsorbing shale reservoir. For each case, the intercept on the x-axis indicates the predicted OGIP of the reservoir. It can be seen that adsorption increases the gas storage capacity and, accordingly, the amount of recoverable gas reserves. The increase correlates positively with initial reservoir pressure, as a result of increased bulk gas density *and* adsorption. Yet, the characteristic shape of the Langmuir isotherm (Figure 1) further indicates that the gain in OGIP brought by adsorption relative to the contribution of the dense bulk phase diminishes with increasing P_0; for example, at a P_0 of 5 MPa, the OGIP is 119% higher than the volumetric reservoir, while at a P_0 of 35 MPa, the same difference is reduced to 13%.

For $P_0 = 5$ MPa and 10 MPa, the "absolute" and "excess" scenarios outline a similar behaviour relative to the base case, while indicating larger recoverable volumes over the entire operating range of pressures. For larger values of P_0, the "absolute" curve continues to stay on the right-hand side of the trend indicated by

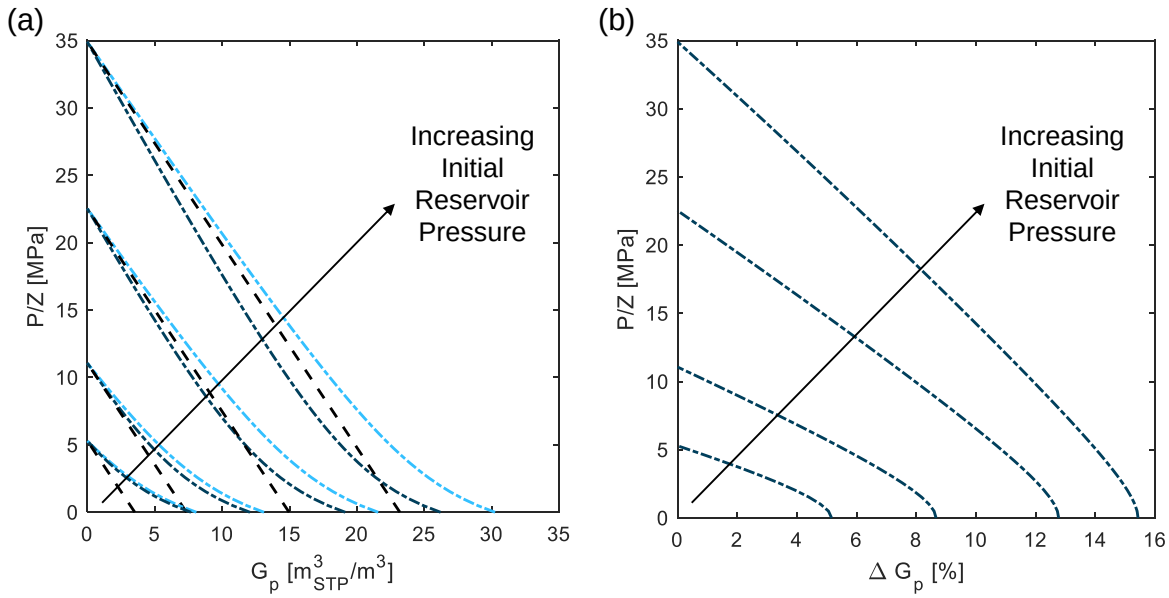

Figure 3: (a) CH_4 cumulative gas production (G_p) as a function of P/Z for four initial reservoir pressures ($P_0 = 5, 10, 20, 35$ MPa) and three scenarios, namely no adsorption (dashed straight line); adsorption without porosity correction (light blue); and adsorption with porosity correction (dark blue). Adsorption is described with a Langmuir isotherm model (parameters given in the Supplementary Information). (b) The relative difference, ΔG_p, between the two adsorption scenarios as a function of P/Z for the same initial reservoir pressures as in (a).

the base case (black line). On the contrary, the "excess" curve follows a path on the left-hand side of the base case, before crossing it, when the pressure is sufficiently low. This behaviour nicely shows the effect of the reduction in pore-space due to the presence of the adsorbed phase − the latter decreases the contribution from the decompression of the free-gas that drives the initial stages of production for deep reservoirs. As discussed further below, this observation indicates that while adsorption does increase the OGIP, it does not necessarily sustain a larger gas production, and that careful consideration needs to be given to the type of adsorption isotherm and the initial reservoir pressure.

At $P_0 = 35$ MPa, both the "absolute" OGIP (30.2 m^3_{STP}/m^3) and "excess" OGIP (26.2 m^3_{STP}/m^3) are larger than the OGIP for the "base case" (23.2 m^3_{STP}/m^3). However, the predicted enhancement is significantly different (30% vs. 13%). Ambrose et al. (2012) demonstrated that the total gas storage capacity decreases between 10–25% when the adsorbed volume is duly considered [27]. Here, we extend this analysis by considering the entire gas production curve − from the initial pressure to any selected abandonment pressure. This is shown in Figure 3b, where the relative difference between the production curves predicted by the two adsorption scenarios ("absolute" and "excess") is plotted for the four initial reservoir pressures. It can be seen that the overestimation for production starting at $P_0 = 5$ MPa is rather limited; the maximum

deviation is about 5%. As the initial reservoir pressure rises, this discrepancy increases, and at $P_0 = 35$ MPa, the OGIP is overestimated by approximately 15% using the incorrect adsorption framework.

We note that the GIP calculations presented above are based on a fairly large set of parameters, as outlined in Section 3.2. While the observed trends are quite general, the relative strength of the overestimation will depend on the specific values of reservoir porosity and adsorption isotherm parameters. A sensitivity analysis for these parameters is presented in the Supplementary Information.

4.1.2. GIP and Adsorption Isotherm Model

Cumulative gas production curves obtained using the four different adsorption isotherm models are shown in Figure 4a for $P_0 = 35$ MPa. For a given value of P/Z, G_p increases in the order Langmuir $<$ Linear $\approx$ BET $<$ Anti-Langmuir, mirroring the order observed for the excess adsorption isotherms (Figure 1a). The higher the excess adsorption at a given pressure, the stronger is the reduction in the available pore space for the free gas and, accordingly, in the enhancement of recoverable gas. With the exception of the Langmuir case, the curves obtained for all the isotherm models are on the right-hand side of curve describing the base case, indicating larger cumulative recovery right from the start of gas production. This behaviour can be traced back to the definition of excess adsorption and is again reflected in the characteristic shape of the excess adsorption isotherm, which may or may not show a maximum. The presence of a maximum (Langmuir case) is an indication that a threshold pressure (or P/Z value) has been reached beyond which the increase in mass stored by adsorption is less than the corresponding increase by simple gas compression. In practical terms, beyond this point the formation of the adsorbed phase reduces the potential for gas storage; in a scenario of primary recovery this translates into less gas being produced compared to a non-adsorbing reservoir with the same porosity. This apparent smaller gas production continues until the pressure is reduced below the threshold value; here, the G_p curve crosses the "base-case" in Figure 4a and the desorbed gas provides the expected enhancement in gas production. This ability to map the characteristic shape of the excess adsorption isotherm to the cumulative gas production curve highlights the importance of accurate adsorption data for the design of a primary recovery operation.

Figure 4b shows the relative difference between the G_p obtained from the "absolute" and "excess" scenarios discussed above. The relative difference increases as the reservoir is depressurised, reaching a maximum of approximately 15% at complete reservoir depletion. The different models approach this maximum at different rates, again reflecting the characteristic shape of each adsorption isotherm. These observations further indicate that at a given production pressure the overestimation brought by the incorrect use of absolute

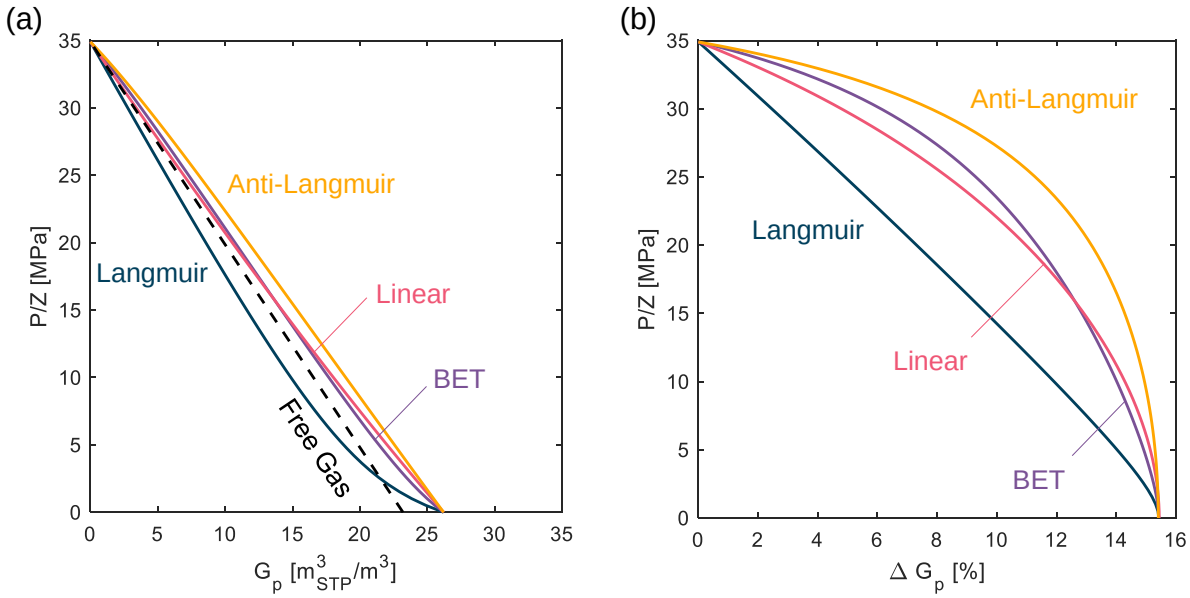

Figure 4: (a) CH_4 cumulative gas production (G_p) as a function of P/Z computed using for different adsorption models in the excess formulation and their comparison with the "base case" (dashed black line, no adsorption). (b) The corresponding relative difference, ΔG_p, between the two adsorption scenarios "absolute" and "excess" as a function of P/Z.

adsorption in GIP calculations depends not only on the extent of adsorption, but also on the shape of the adsorption isotherm.

4.2. Recovery with Gas Injection

4.2.1. Process Description

The operation of the enhanced recovery process that cycles between Injection, Soak and Production steps is represented in Figure 5a,b for the case of CO_2 injection and in Figure 5c,d for the case of N_2 injection. Each cycle is depicted by three symbols of the same colour, with the exception of 'Cycle 0' that includes only the transition from the initial state of the reservoir ($y^0_m = 1$, $P_0 = 35$ MPa) to $P_L = 10$ MPa (these points are shown in grey). The transition between each state and cycle (the operating line) is indicated by the black arrows. The reservoir's final state is represented by the yellow point, which is the result of a final Soak after the last Production stage. The competitive absolute adsorption isotherms at various equilibrium compositions (y^S_m or $1 - y^S_m$) at the Soak stage are also shown in each plot. These have been obtained from the extended Langmuir adsorption isotherm model. We note that the methane adsorption parameters used for this case study differ from those used in the previous section (see Supplementary Information).

As an example of general validity, the first cycle of the CO_2-ESGR operation is discussed first (red symbols in Figures 5a and 5b). The reservoir has been depressurised to $P_L = 10$ MPa, followed by the injection of

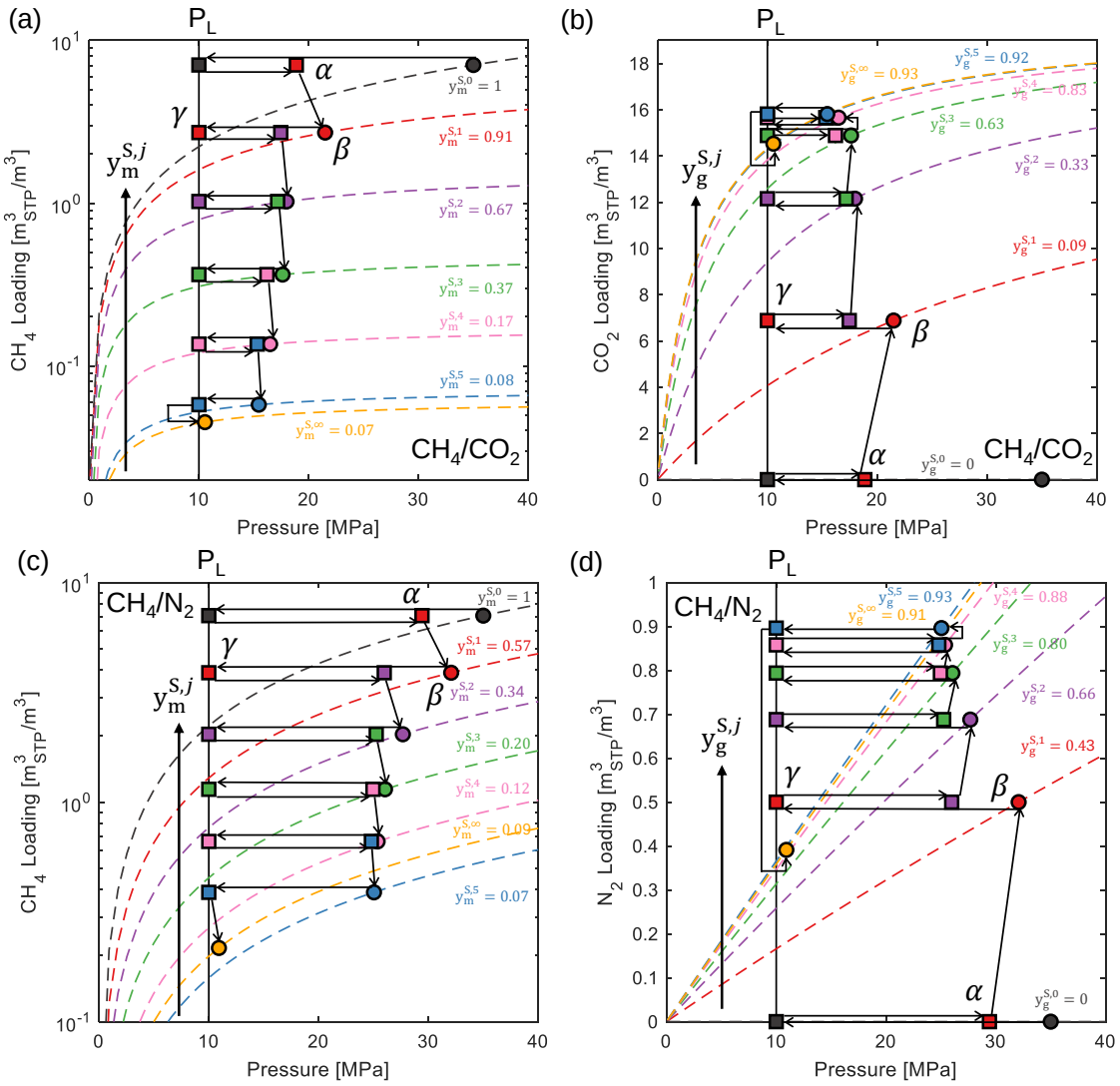

Figure 5: Transitions (black arrows) during the cyclic CH_4 recovery with gas injection by either CO_2 (a,b) or N_2 (c,d). The results are plotted as absolute adsorption loadings for each gas and the dashed lines indicate the competitive loadings at the equilibrium composition in the Soak stages ($y_i^{S,j}$). The superscripts '0' and '∞' represent the initial and abandoned reservoir conditions representatively. The symbols α, β and γ represent the Injection, Soak and Production stage for the first cycle. P_L refers to the production pressure and each cycle is illustrated by a different colour.

CO_2 (state α), which raises the reservoir pressure to approximately 21 MPa. During the Soak stage (state β), the composition of the bulk gas changes, as a result of the equilibration with the adsorbed phase, reaching a final value $y_{\mathrm{m}}^{\mathrm{S}} = 0.91$. It should be noted that this point lies on the corresponding equilibrium adsorption isotherm (dashed line). The reservoir is then depressurised to $P_{\mathrm{L}} = 10$ MPa (state γ) by producing a gas mixture with composition $y_{\mathrm{m}} = 0.91$. Thereafter, a new cycle starts by re-introducing CO_2 in the reservoir. Through the sequence of cycles, the symbols in Figure 5a (CH_4 loading) move downwards, while those in Figure 5b (CO_2 loading) move upwards, meaning that the reservoir is being depleted in CH_4 and enriched in CO_2. After five cycles, the bulk gas composition has reached a value $y_{\mathrm{m}} = 0.08$.

In the case of N_2 injection (Figures 5c and 5d), the pressure swing is much wider, reaching a pressures as high as 32 MPa at the end of the first injection step (state α). The higher N_2 partial pressure leads to an equally strong reduction in the CH_4 loading already after the first Soak stage (state β, 3.9 $\mathrm{m}^3_{\mathrm{STP}}/\mathrm{m}^3$ vs. 2.7 $\mathrm{m}^3_{\mathrm{STP}}/\mathrm{m}^3$ with CO_2), albeit with a produced gas that is leaner in CH_4 (state γ, $y_{\mathrm{m}} = 0.57$ vs. $y_{\mathrm{m}} = 0.91$ with CO_2). The lower concentration of CH_4 in the gas phase is the result of the unfavourable adsorption competition, as CH_4 has a stronger affinity for the shale than N_2, while the opposite is true for CO_2/CH_4 mixtures. These observations indicate that partial pressure and competitive adsorption both act towards enhancing gas production, but they do so in complementary ways. The final reservoir pressure after the N_2-ESGR is 11 MPa, similar to the CO_2 injection scenario, but the amount of adsorbed CH_4 remaining in the reservoir is slightly more (0.2 $\mathrm{m}^3_{\mathrm{STP}}/\mathrm{m}^3$ vs. 0.05 $\mathrm{m}^3_{\mathrm{STP}}/\mathrm{m}^3$ with CO_2). The reservoir is abandoned with a N_2 loading of approximately 0.4 $\mathrm{m}^3_{\mathrm{STP}}/\mathrm{m}^3$ ($y_{\mathrm{m}} = 0.09$), as compared to the approximately 15 $\mathrm{m}^3_{\mathrm{STP}}/\mathrm{m}^3$ of adsorbed CO_2 left in the reservoir after the CO_2-ESGR operation ($y_{\mathrm{m}} = 0.08$).

4.2.2. State of the Reservoir

A better understanding of the mechanisms driving the recovery of CH_4 in the two ESGR scenarios is achieved by analysing the evolution of both the FG (y_i) and the AG (z_i) composition. Here, we will additionally consider the partitioning of each gas between the FG and AG, as given by:

$$f_i = \frac{n_{i,\mathrm{a}}}{N_{i,\mathrm{t}}} \tag{22}$$

for methane and $1 - f_i$ for the injected species (CO_2 or N_2). Figure 6 illustrates these different ratios for (a) CO_2-ESGR and (b) N_2-ESGR; in each plot, the lines indicate the variation of these quantities with each Soak stage and the symbols represent the Soak after the last Production stage.

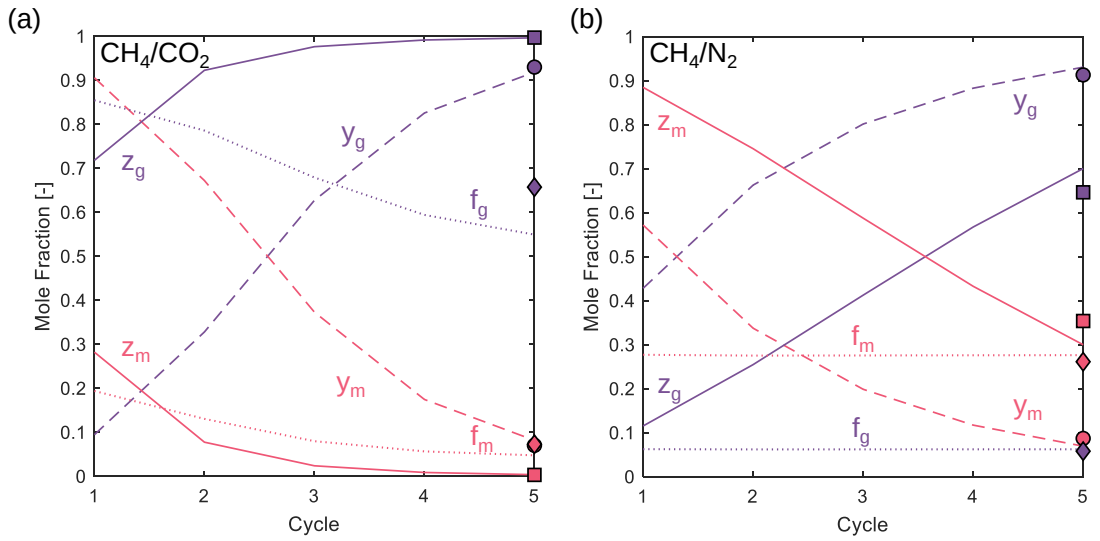

Figure 6: Evolution of the composition of both the adsorbed and bulk phase after each soak stage for the (a) CH_4/CO_2 and (b) CH_4/N_2 ESGR scenarios. CH_4 is shown in pink, while the injected gas is shown in purple. Lines indicate the change in mole fractions at each cycle (at the Soak stage), while the symbols indicate the final state of the reservoir (at the final Soak after the last Production stage). Solid lines and squares indicate z_i (adsorbed phase); dashed lines and circles indicate y_i (bulk phase); dotted lines and diamonds indicate f_i (fraction of adsorbed phase).

While they are qualitatively similar, the trends outlined by the two injection schemes show important differences. Across cycles, the fraction f_i of each component is fairly constant (dotted lines), with CH_4 remaining below 30% for both schemes; however, for the injected gas $f_g \approx 55$–$85\% > f_m$ for CO_2-ESGR and $f_g \approx 6\% < f_m$ for N_2-ESGR, highlighting the opposite adsorption selectivity of these two gases relative to CH_4. This ordering applies also after completion of the cyclic operation: the diamond symbols show that 7–26% of the total amount of methane is in the AG phase, whereas 66% and 6% of the total amount of CO_2 and N_2 remains in the AG phase, respectively. In terms of phase composition (solid lines), the AG is dominated by CH_4 in the early N_2-ESGR cycles, with a crossover after Cycle 3; on the contrary, $z_m \approx 0.3$ already at Cycle 1 for CO_2-ESGR and the AG becomes richer in CO_2 at every cycle, reaching a value $z_g \approx 1$ after 5 cycles ($z_g \approx 0.6$ for N_2). As discussed above, this apparent inefficiency of N_2 to extract CH_4 by adsorption is compensated by the stronger reduction in CH_4 partial pressure, relative to the CO_2 injection scenario. This behaviour is confirmed by the trends outlined by the gas phase composition, y_i (dashed lines). In both scenarios, the bulk phase is initially richer in CH_4 ($y_m \approx 0.91$ for CO_2 and $y_m \approx 0.57$ for N_2), with a crossover appearing already after Cycle 1 for N_2-ESGR and only after Cycle 2 for CO_2-ESGR. When the two processes are compared, it can be seen that y_g is always greater with N_2 rather than CO_2.

4.2.3. Performance Evaluation

The CO_2-ESGR and N_2-ESGR operations are compared in Figure 7 by considering the total volume of CH_4 produced, as well as the volume of gas (CO_2 or N_2) injected and stored in the reservoir, which are evaluated in terms of incremental and cumulative amounts. Both scenarios start with an initial depressurisation from P_0 to P_L (Cycle 0), which produces 12.2 m^3_{STP}/m^3 of CH_4. Thereafter, the same amount of gas is introduced in each cycle (8 m^3_{STP}/m^3), for a total of 40 m^3_{STP}/m^3 of gas injected. After five cycles, approximately 26 m^3_{STP}/m^3 of CH_4 have been recovered for both CO_2- and N_2-ESGR. In both cases, the first depressurisation contributes to about 48% of the total recovery and the first two cycles prove to be the most effective in terms of recovery and storage. By the end of Cycle 2, 85% and 87% of the total recovery has been achieved for CO_2- and N_2-ESGR, respectively. The volume of gas stored after five cycles amounts to 22 m^3_{STP}/m^3 (CO_2) and 7 m^3_{STP}/m^3 (N_2); 63% and 71% of this amount is stored by the end of Cycle 2, respectively.

Prior to the start of the ESGR operation, there is only methane in the reservoir and approximately 27% of this mass is found as adsorbed gas. Methane contribution to the GIP reduces to approximately 63% after the first injection, irrespective of the injected gas, and to approximately 3% and 11%, at the end of the operation for CO_2 and N_2, respectively. For CO_2-ESGR, the AG contribution to the GIP increases to an average of 53%, reaching 64% at the end of the operation. The opposite behaviour is observed for N_2-ESGR, whereby the AG contribution to the GIP decreases to an average of 13% during the Soak stages, reaching 8% at the final reservoir pressure. These numbers reflect both the removal of CH_4 from the system as well as the preferential retention of CO_2 in the adsorbed phase. On a volume basis, the AG occupies initially 17% of the total porosity and this value increases to approximately 37% at the final reservoir condition during CO_2-ESGR. On the contrary, when N_2 is used, the fraction of porosity occupied by the AG decreases to 11% after the first cycle and reaches a value of only 1% in the final state. The reservoir is now by and large a "conventional" reservoir, where most of the gas is found as compressed gas.

5. Discussion

This section will focus on a strategy for (i) primary recovery and (ii) recovery with gas injection, based on the observations in the previous section.

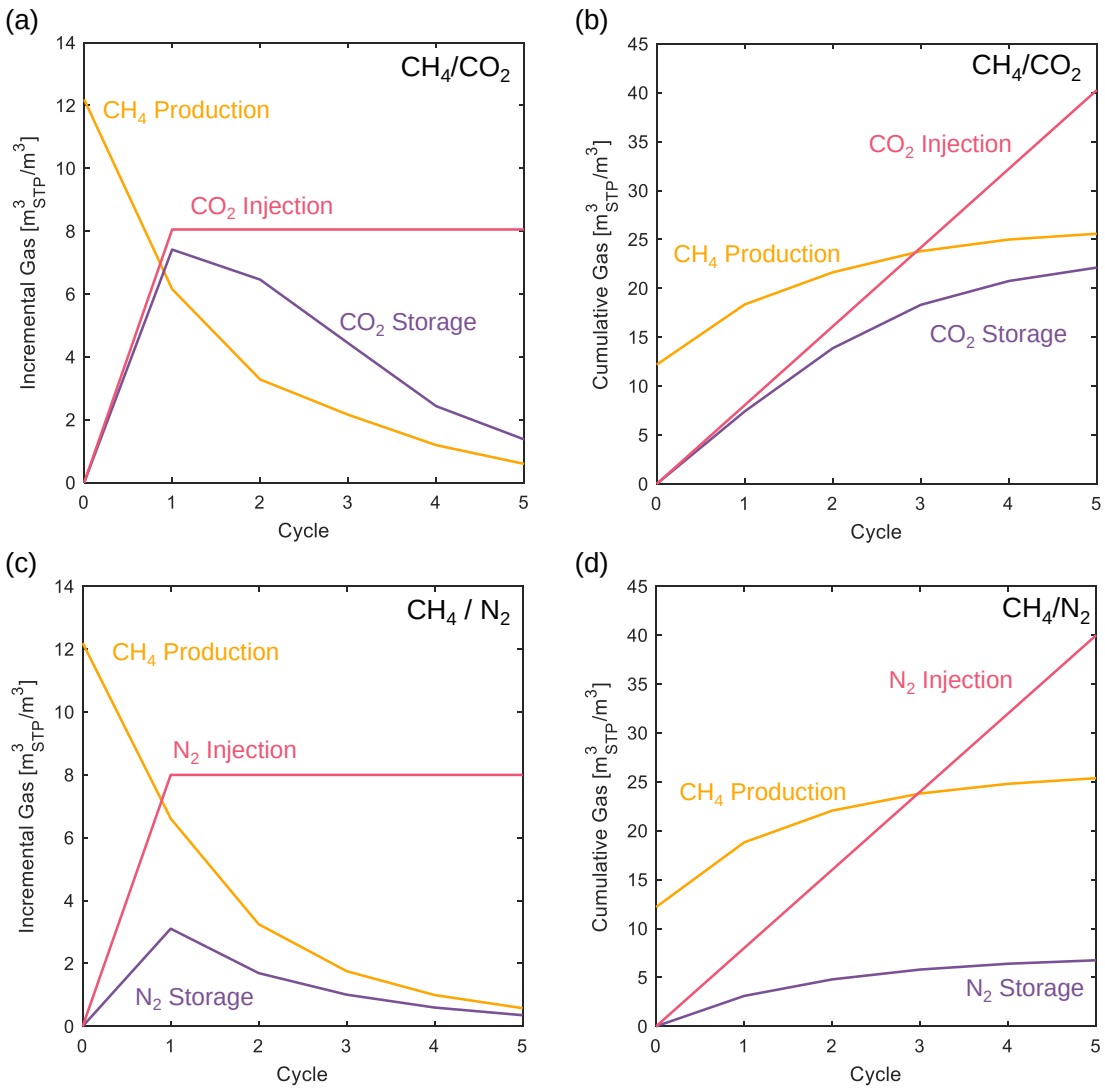

Figure 7: Incremental and cumulative volume of gas injected, stored and CH_4 produced for each cycle during the ESGR operation driven by CO_2 (a,b) and N_2 (c,d) injection. 'Cycle 0' refers to the depressurisation of the reservoir from the initial pressure to the production pressure, P_L.

5.1. Strategy for Primary Recovery

The sensitivity of the $G_p - P/Z$ curve to the selected adsorption isotherm model provides scope for identifying a suitable strategy for primary recovery. The inverse of the slope of the curves depicted in Figures 3a and 4a can be interpreted as a 'production rate' - the amount of gas produced within each incremental change in P/Z. While in the absence of adsorption ("base case") this production rate is constant, the non-linearity introduced by the desorption process is such that this rate depends on pressure. It was already anticipated in Section 4.1 that the Langmuir isotherm can lead to initial production rates that are lower than

those estimated based on total porosity alone. This is typically the case for deep reservoirs (high P_0), which would therefore require fairly low production pressures to observe the desired enhancement brought by the desorbing gas. For two of the cases depicted in Figure 3a, the production rates for an adsorbing reservoir are always higher than the volumetric reservoir (P_0 = 5 MPa and 10 MPa). At a P_0 of 20 MPa or 35 MPa, the same is only true below a production pressure of approximately 11 MPa . These initial considerations have implications in the planning of the primary recovery operation and in the selection of an abandonment pressure.

In general terms, reservoir production continues until declining production rates cause it to be no longer economically viable [54]. In this context, a shale that shows adsorption data following an Anti-Langmuir isotherm represents the most favourable option, because it has the highest gas production rate right at the start of production (see again Figure 4a). Accordingly, a process designed to produce a given amount of gas (G_p) would result in a higher abandonment pressure compared to the value required for an equivalent shale reservoir described with the other adsorption isotherms. For a shale that shows a linear adsorption isotherm, the production rate would increase linearly with the depressurisation of the reservoir. The characteristic shape of the BET adsorption isotherm model leads to a production scenario that share similarities with the Anti-Langmuir and Langmuir cases, which enable maintaining fairly high production rate throughout the entire pressure range. Based on this analysis, to achieve a given value of G_p, the abandonment pressures of the reservoirs would be in the order P(AL) > P(Lin) > P(BET) > P(L). Because of the fairly low abandonment pressure associated with a shale characterised by a Langmuir-type adsorption isotherm, a production strategy that involves the injection of a sweep gas is advisable, as discussed in the next section.

5.2. Strategy for Recovery with Gas Injection

The CO_2 and N_2-ESGR strategies studied in this work can be evaluated on the basis of the performance metrics shown in Table 3.

Table 3: Performance metrics estimated from the Shortcut Pressure Swing Adsorption Analogue Model using CO_2 and N_2 injection to enhance CH_4 recovery. The Enhanced Recovery (R_m) and Storage (S_g) factors are defined by Eqs. 20 and 21, respectively.

Parameter	CO_2	N_2
R_m	150%	149%
S_g	54.9%	16.9%
Primary Recovery	65.0%	
Recovery with Gas Injection	97.6%	96.8%

Primary recovery results in extraction of only 65% of the CH_4 in the reservoir, while production using CO_2 or N_2 yields a methane recovery of 97.6% and 96.8%, respectively. The corresponding increase relative to the primary recovery is thus approximately $R_m = 150\%$. As discussed above, for CO_2 this is primarily due to favourable competitive adsorption, while for N_2 the primary mechanism is the strong reduction in CH_4 partial pressure associated with the wider pressure swing. To produce the same volume of CH_4 without any gas injection, the reservoir would have to be depressurised to about 0.5 MPa. This pressure is thus much lower than the production pressure sustained during the ESGR operation ($P_L = 10$ MPa). For the reservoir to have the same final absolute adsorbed amount of CH_4 as the reservoir with CO_2 or N_2 storage, primary recovery would result in depressurisation to below 1 MPa. A key advantage of CO_2-ESGR is the storage of CO_2 and the consequent environmental benefit; approximately half of the injected CO_2 is effectively stored ($S_g = 54.9\%$) and 66% of this CO_2 is adsorbed. For N_2, $S_g = 16.9\%$ and 6% of this amount is adsorbed. Simulation studies reported in the literature indicate similar trends in terms of recovery and storage [55]. Others propose to inject a mixture of the two gases [56], although this potentially lowers the CO_2 storage potential of the shale reservoir. Most notably, the results obtained with our simplified model compare favourably with observations from a field operation [17]. In the latter case, a single CO_2 injection cycle was completed that enabled the increase of hydrocarbon production by 2–3 times (compared to the forecasted production by primary recovery), while storing approximately 60% of the injected CO_2. The field study concluded that larger recovery factors could have been achieved upon increasing the volume of CO_2 injected and its pressure. As shown in this study, one strategy to achieve this goal is to carry out additional injection (and soak) cycles.

Figure 8 shows the cumulative and incremental changes of performance metrics reported in Table 3 (R_m and S_g) as a function of each cycle for both (a) CO_2- and (b) N_2-ESGR. The trends observed for both systems are very similar, with N_2 sustaining a slightly lower level of production at every cycle. It can also be seen that initial depressurisation (Cycle 0) contributes greatly to the total recovery (48% of the total CH_4 recovered using either CO_2 or N_2). The total pressure of the reservoir for CO_2-ESGR oscillates between 10 MPa (the production pressure, P_L) and the pressure after the Injection and Soak stages, which is between 15–21 MPa. For N_2-ESGR, the pressure increase is up to 25–32 MPa with gas injection; as discussed above, the wider pressure swing compensates for the unfavourable competitive adsorption of the N_2/CH_4 system. Accordingly, more CH_4 could be produced by CO_2-ESGR if a higher Injection/Soak pressure could be obtained using a higher volume of CO_2 injected per cycle. As discussed above, CO_2 leads also to significantly larger storage

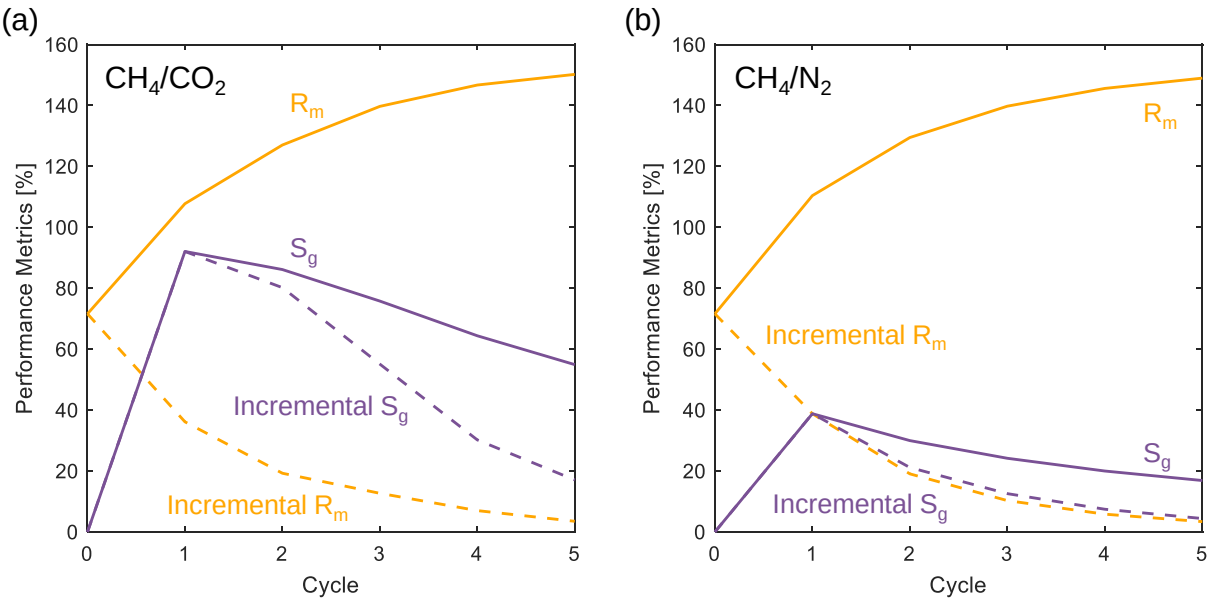

Figure 8: The performance metrics as a function of each injection cycle for the (a) CH_4/CO_2 and (b) CH_4/N_2 systems. Both R_m and S_g, which are cumulative quantities, are shown as solid lines and incremental quantities, i.e. metrics that are based solely on each cycle, are shown as dashed lines. 'Cycle 0' refers to the initial depressurisation of the reservoir where there is no gas injection.

than N_2, the majority of which is already achieved during the first cycle.

The Enhanced Recovery and Storage factors discussed above should be regarded as theoretical maxima, because they are based on complete equilibrium being achieved at the Soak stages. Realistically, this might take a significant amount of time, which might not be economical. We also note that more than half of the CO_2 injected is produced, and there will be some cost associated with its separation from the produced CH_4 before its reinjection into the reservoir. An optimisation strategy that prioritises CO_2 storage and CH_4 recovery, without compromising the purity of the produced stream, is required. Similar considerations apply to N_2-ESGR, but with a heavier burden on the economics of the operation, given that there is no real incentive in storing N_2.

6. Conclusion

We have analysed shale gas production from primary and secondary recovery with gas injection using material balance calculations that correctly account for the reduction in the the available porosity due to gas adsorption. While previous work has shown that the OGIP is overestimated if the adsorbed volume is not duly considered, we have extended here the analysis to the entire gas production curve – from the initial

pressure to any selected abandonment pressure. In this endeavour, we have shown that adsorption does not necessarily sustain a larger gas production relative to a non-adsorbing reservoir with the same porosity, and that careful consideration needs to be given to the initial reservoir pressure and the type of adsorption isotherm. The latter can significantly impact the strategy used for primary or recovery with gas injection.

The shortcut Pressure Swing Adsorption analogue model developed in this work provides a practical way to test injection strategies for ESGR. We evaluated CO_2 and N_2 and observed that (i) they are both equally successful at enhancing recovery of CH_4 and (ii) they exploit different means to achieve this (competitive adsorption and partial pressure reduction, respectively). In N_2-ESGR, the volume of N_2 stored is less than half of the volume of CO_2 stored. This further indicates that more N_2 is being produced with natural gas, leading to higher separation costs. In CO_2-ESGR, about half of the CO_2 injected is stored in the reservoir, meaning that the operation may be both economically and environmentally attractive. Yet, as CO_2 increases in the system, the benefit gained by the recovery process might be offset by the costs involved in maintaining the injection of CO_2, as a lot of the CH_4 has already left the system. Various injection strategies could be explored in the future, whereby the injection volume is gradually reduced with each cycle.

The soaking stage represents a key element of the cyclic operation, because it is where adsorption equilibrium is attained. In our model formulation we did not consider the time to reach this equilibrium, although this represents a key aspect of shale gas production. The dynamics of adsorption/desorption and the consequences of not waiting for true equilibrium to be achieved are topics for further study. We envisage that current production strategies that use several lateral wells could be exploited also for ESGR, whereby each well undergoes alternately injection, soaking and production. In this context, the proposed proxy model could be exploited to identify optimum strategies to operate such a multi-well system.

Acknowledgements

The authors acknowledge the funding provided by the Commonwealth Scientific and Industrial Research Organisation (CSIRO). HA thanks the Marit Mohn Scholarship at Imperial College London. LJ thanks the BP International Centre for Advanced Materials for support through a Kathleen Lonsdale research fellowship.

References

[1] IEA. World energy outlook 2019. Report, IEA, 2019.

[2] M. Melikoglu. Shale gas: Analysis of its role in the global energy market. *Renewable and Sustainable Energy Reviews*, 37:460–468, 2014.

[3] Q. Wang, X. Chen, A. N. Jha, and H. Rogers. Natural gas from shale formation the evolution, evidences and challenges of shale gas revolution in united states. *Renewable and Sustainable Energy Reviews*, 30:1–28, 2014.

[4] J. Cooper, L. Stamford, and A. Azapagic. Shale gas: A review of the economic, environmental, and social sustainability. *Energy Technology*, 4(7):772–792, 2016.

[5] R. Pini. Assessing the adsorption properties of mudrocks for CO2 sequestration. *Energy Procedia*, 63:5556–5561, 2014.

[6] X. Cui, A. M. M. Bustin, and R. M. Bustin. Measurements of gas permeability and diffusivity of tight reservoir rocks: different approaches and their applications. *Geofluids*, 9(3):208–223, 2009.

[7] B. K. Sovacool. Cornucopia or curse? Reviewing the costs and benefits of shale gas hydraulic fracturing (fracking). *Renewable and Sustainable Energy Reviews*, 37:249–264, 2014.

[8] EIA. Technically recoverable shale oil and shale gas resources: An assessment of 137 shale formations in 41 countries outside the united states. Report, EIA, 2013.

[9] R. Sandrea and I. Sandrea. New well-productivity data provides US shale potential insights. *Oil & Gas Journal*, 112(11), 2014.

[10] R. Pini, G. Storti, and M. Mazzotti. A model for enhanced coal bed methane recovery aimed at carbon dioxide storage. *Adsorption*, 17(5):889–900, 2011.

[11] M. Godec, G. Koperna, R. Petrusak, and A. Oudinot. Potential for enhanced gas recovery and CO2 storage in the marcellus shale in the eastern united states. *International Journal of Coal Geology*, 118:95–104, 2013.

[12] X. Li and D. Elsworth. Geomechanics of CO2 enhanced shale gas recovery. *Journal of Natural Gas Science and Engineering*, 26:1607–1619, 2015.

[13] Z. Tao and A. Clarens. Estimating the carbon sequestration capacity of shale formations using methane production rates. *Environmental Science & Technology*, 47(19):11318–11325, 2013.

[14] R. Xu, K. Zeng, C. Zhang, and P. Jiang. Assessing the feasibility and CO2 storage capacity of CO2 enhanced shale gas recovery using triple-porosity reservoir model. *Applied Thermal Engineering*, 115:1306–1314, 2017.

[15] M. Godec, G. Koperna, R. Petrusak, and A. Oudinot. Enhanced gas recovery and CO2 storage in gas shales: A summary review of its status and potential. *Energy Procedia*, 63:5849–5857, 2014.

[16] R. W. J. Edwards, M. A. Celia, K. W. Bandilla, F. Doster, and C. M. Kanno. A model to estimate carbon dioxide injectivity and storage capacity for geological sequestration in shale gas wells. *Environmental Science & Technology*, 49(15):9222–9229, 2015.

[17] K. Louk, N. Ripepi, K. Luxbacher, E. Gilliland, X. Tang, C. Keles, C. Schlosser, E. Diminick, S. Keim, J. Amante, and K. Michael. Monitoring CO2 storage and enhanced gas recovery in unconventional shale reservoirs: Results from the morgan county, tennessee injection test. *Journal of Natural Gas Science and Engineering*, 45:11–25, 2017.

[18] P. Charoensuppanimit, S. A. Mohammad, and K. A. M. Gasem. Measurements and modeling of gas adsorption on shales. *Energy & Fuels*, 30(3):2309–2319, 2016.

[19] S. Merey and C. Sinayuc. Analysis of carbon dioxide sequestration in shale gas reservoirs by using experimental adsorption data and adsorption models. *Journal of Natural Gas Science and Engineering*, 36, Part A:1087–1105, 2016.

[20] R. J. Ambrose, R. C. Hartman, M. Diaz-Campos, I. Y. Akkutlu, and C. Sondergeld. New pore-scale considerations for shale gas in place calculations, 2010.

[21] A. Leahy-Dios, M. Das, A. Agarwal, and R. D. Kaminsky. Modeling of transport phenomena and multicomponent sorption for shale gas and coalbed methane in an unstructured grid simulator, 2011.

[22] F. Hao, H. Zou, and Y. Lu. Mechanisms of shale gas storage: Implications for shale gas exploration in China. *AAPG bulletin*, 97(8):1325–1346, 2013.

[23] C. M. Freeman, G. J. Moridis, D. Ilk, and T. A. Blasingame. A numerical study of performance for tight gas and shale gas reservoir systems, 2009.

[24] K. Bruner and R. Smosna. A comparative study of the mississippian barnett shale, fort worth basin, and devonian marcellus shale, appalachian basin. Report, National Energy Technology Laboratory (NETL), US Department of Energy (USDOE), 2011.

[25] T. F. T. Rexer, M. J. Benham, A. C. Aplin, and K. M. Thomas. Methane adsorption on shale under simulated geological temperature and pressure conditions. *Energy & Fuels*, 27(6):3099–3109, 2013.

[26] S. M. Kang, E. Fathi, R. J. Ambrose, I. Y. Akkutlu, and R. F. Sigal. Carbon dioxide storage capacity of organic-rich shales. *SPE Journal*, 16(04), 2011.

[27] R. J. Ambrose, R. C. Hartman, M. Diaz-Campos, I. Y.l Akkutlu, and C. H. Sondergeld. Shale gas-in-place calculations part I: New pore-scale considerations. *SPE Journal*, 17(01):219–229, 2012.

[28] D. Silin and T. J. Kneafsey. Shale gas: Nanometer-scale observations and well modelling. *Journal of Canadian Petroleum Technology*, 51(06):464–475, 2012.

[29] R. Pini. Interpretation of net and excess adsorption isotherms in microporous adsorbents. *Microporous and Mesoporous Materials*, 187:40–52, 2014.

[30] P. Chareonsuppanimit, S. A. Mohammad, R. L. Robinson, and K. A. M. Gasem. High-pressure adsorption of gases on shales: Measurements and modeling. *International Journal of Coal Geology*, 95:34–46, 2012.

[31] M. Gasparik, A. Ghanizadeh, P. Bertier, Y. Gensterblum, S. Bouw, and B. M. Krooss. High-pressure methane sorption isotherms of black shales from the Netherlands. *Energy & Fuels*, 26(8):4995–5004, 2012.

[32] T. Zhang, G. S. Ellis, S. C. Ruppel, K. Milliken, and R. Yang. Effect of organic-matter type and thermal maturity on methane adsorption in shale-gas systems. *Organic Geochemistry*, 47:120–131, 2012.

[33] M. Gasparik, T. F. T. Rexer, A. C. Aplin, P. Billemont, G. De Weireld, Y. Gensterblum, M. Henry, B. M. Krooss, S. Liu, X. Ma, R. Sakurovs, Z. Song, G. Staib, K. M. Thomas, S. Wang, and T. Zhang. First international inter-laboratory comparison of high-pressure CH4, CO2 and C2H6 sorption isotherms on carbonaceous shales. *International Journal of Coal Geology*, 132:131–146, 2014.

[34] J. Schell, N. Casas, R. Pini, and M. Mazzotti. Pure and binary adsorption of CO2, H2, and N2 on activated carbon. *Adsorption*, 18(1):49–65, 2012.

570 [35] M. Sudibandriyo, Z. Pan, J. E. Fitzgerald, R. L. Robinson, and K. A. M. Gasem. Adsorption of methane,
571 nitrogen, carbon dioxide, and their binary mixtures on dry activated carbon at 318.2 K and pressures
572 up to 13.6 MPa. *Langmuir*, 19(13):5323–5331, 2003.

573 [36] K. S. Walton and D. S. Sholl. Predicting multicomponent adsorption: 50 years of the ideal adsorbed
574 solution theory. *AIChE Journal*, 61(9):2757–2762, 2015.

575 [37] V. S. Balashankar, A. K. Rajagopalan, R. de Pauw, A. M. Avila, and A. Rajendran. Analysis of a
576 batch adsorber analogue for rapid screening of adsorbents for postcombustion CO2 capture. *Industrial*
577 *& Engineering Chemistry Research*, 58(8):3314–3328, 2019.

578 [38] V. Pranesh. Subsurface CO2 storage estimation in Bakken tight oil and Eagle Ford shale gas condensate
579 reservoirs by retention mechanism. *Fuel*, 215:580–591, 2018.

580 [39] T. Wan and Z. Mu. The use of numerical simulation to investigate the enhanced Eagle Ford shale gas
581 condensate well recovery using cyclic CO2 injection method with nano-pore effect. *Fuel*, 233:123–132,
582 2018.

583 [40] R. Iddphonce, J. Wang, and L. Zhao. Review of CO2 injection techniques for enhanced shale gas
584 recovery: Prospect and challenges. *Journal of Natural Gas Science and Engineering*, 77:103240, 2020.

585 [41] J. S. Levine, I. Fukai, D. J. Soeder, G. Bromhal, R. M. Dilmore, G. D. Guthrie, T. Rodosta, S. Sanguinito,
586 S. Frailey, C. Gorecki, W. Peck, and A. L. Goodman. U.S. DOE NETL methodology for estimating the
587 prospective CO2 storage resource of shales at the national and regional scale. *International Journal of*
588 *Greenhouse Gas Control*, 51:81–94, 2016.

589 [42] S. Moghadam, O. Jeje, and L. Mattar. Advanced gas material balance in simplified format. *Journal of*
590 *Canadian Petroleum Technology*, 50(01):90–98, 2011.

591 [43] E. W. Lemmon, M. L. Huber, and M. O. McLinden. NIST standard reference database 23: Reference
592 fluid thermodynamic and transport properties-REFPROP, version 10.0, 2018.

593 [44] D. M. Kargbo, R. G. Wilhelm, and D. J. Campbell. Natural gas plays in the Marcellus shale: Challenges
594 and potential opportunities. *Environmental Science & Technology*, 44(15):5679–5684, 2010.

595 [45] EIA. U.S. crude oil and natural gas proved reserves, year-end 2018. Report, EIA, 2019.

[46] P. Weniger, W. Kalkreuth, A. Busch, and B. M. Krooss. High-pressure methane and carbon dioxide sorption on coal and shale samples from the Paraná basin, Brazil. *International Journal of Coal Geology*, 84(3-4):190–205, 2010.

[47] R. H. Williams, D. K. Khatri, R. F. Keese, S. L. Roy-Delage, J. M. Roye, D. L. R. Leach, O. Porcherie, P. Rottler, and J. Rodriguez. Flexible, expanding cement system (FECS) successfully provides zonal isolation across marcellus shale gas trends, 2011.

[48] W. Yu, K. Sepehrnoori, and T. W. Patzek. Modeling gas adsorption in Marcellus shale with Langmuir and BET isotherms. *SPE Journal*, 21(2):589600, 2016.

[49] EIA. Review of emerging resources: U.S. gas and shale oil plays. Report, EIA, 2011.

[50] M. L. Boyce, T. R. Carr, T. Carr, T. D'Agostino, W. Ambrose, J. Pashin, and N. C. Rosen. *Lithostratigraphy and Petrophysics of the Devonian Marcellus Interval in West Virginia and Southwestern Pennsylvania*, volume 29, page 0. SEPM Society for Sedimentary Geology, 2009.

[51] P. J. Linstrom and W. G. Mallard. *NIST Chemistry WebBook, NIST Standard Reference Database Number 69*. National Institute of Standards and Technology, Gaithersburg MD, 20899.

[52] R. Heller and M. Zoback. Adsorption of methane and carbon dioxide on gas shale and pure mineral samples. *Journal of Unconventional Oil and Gas Resources*, 8:14–24, 2014.

[53] A. Streb and M. Mazzotti. Adsorption for efficient low carbon hydrogen production: part 2- Cyclic experiments and model predictions. *Adsorption*, 2021.

[54] A. Satter and G. M. Iqbal. *4 - Reservoir fluid properties*, pages 81–105. Gulf Professional Publishing, Boston, 2016.

[55] K. Lin, Q. Yuan, Y.-P. Zhao, and C. Cheng. Which is the most efficient candidate for the recovery of confined methane: Water, carbon dioxide or nitrogen? *Extreme Mechanics Letters*, 9:127–138, 2016.

[56] Z. Li and D. Elsworth. Controls of CO2-N2 gas flood ratios on enhanced shale gas recovery and ultimate CO2 sequestration. *Journal of Petroleum Science and Engineering*, 179:1037–1045, 2019.